High Precision SAR Echo Simulation Based on FDTD Algorithm with Mobile Excitation Source

Shi Qingwu, Zou Bin and Lu Jian
Harbin Institute of Technology
Harbin, China
zoubin@hit.edu.cn;
shiqingwu@126.com;
lujian1995@126.com

***Abstract*—This paper presents a high-precision SAR echo simulation method, which calculates the electromagnetic field distribution of the target with the mobile excitation source using the finite-difference time-domain method (FDTD). Because the RCS of targets is different in different observation periods of different spatial angles, the visual points of targets are divided into continuous equidistant zones according to the relative positions between the target and the excitation source. Based on the near-to-far field extrapolation technology, the far-field values of the local targets are derived from the Huygens surface of the target surface, and the target SAR echo data are finally obtained. Simulation results of typical target show that the method proposed in this paper makes full use of the accuracy of FDTD calculation and truly reflects the backscattering characteristics of the target in different states.**

Keywords—FDTD; SAR echo; mobile excitation source; equidistant zones

I. INTRODUCTION

Synthetic Aperture Radar (SAR) is a kind of all-weather, all-time, high-resolution radar. Its echo signal contains a lot of information such as the size, shape and electromagnetic characteristics of target. Therefore, it is very important to model the SAR working system and simulate the target echo signal. The traditional method accumulates the echo of the whole target according to the echo expression of the single point target which neglects the difference of backscattering characteristic under different observation conditions[1][2]. However, in high-resolution SAR data, especially for angular buildings, the echo data is very angle-sensitive [3]. Therefore, with the development of spaceborne SAR technology and the improvement of resolution, the traditional SAR echo simulation method has been difficult to meet the SAR system design and echo imaging needs. In essence, the SAR echo is the far field scattering signal of the target. The echo of SAR can be simulated as long as finding a method that can accurately acquire the electromagnetic field value of the target in the far field [4]. Based on this idea, K Wang proposed a SAR echo simulation method based on FDTD algorithm, which simulates the physical process of the interaction between the chirp signal sent by the satellite sensor and the target received by the SAR system sensor [5]. However, the time delay of SAR echo signals at different distances and the relationship between moving source and target were not considered fully. Considering the above problems, this paper presents a FDTD algorithm with mobile excitation sources, which can simulate high-precision SAR echo. In reference to the actual working mode of the satellite, a mobile excitation source is established on the satellite orbit. By accurately calculating the location of the mobile excitation source, the sending and receiving process of the SAR signal can be truly simulated. The value of the electric field calculated by the FDTD method can truly reflect the interaction between the electromagnetic wave and the target[6]. Through the near-to-far field transformation of the surface mesh, the details of the scattering of the target are obtained. The calculated RCS and imaging results of the simulated SAR echo data reflect the feasibility and accuracy of the method.

II. MODEL OF MOBILE EXCITATION SOURCE AND TARGET WITH FDTD ALGORITHM

A. Model of Mobile excitation Source and target

In order to simulate the working state of the spaceborne synthetic aperture radar (SAR), the excitation source of the finite difference time domain method is set up in the satellite orbit. As shown in Fig.1, the geometric relationship between the radar and the target is established.

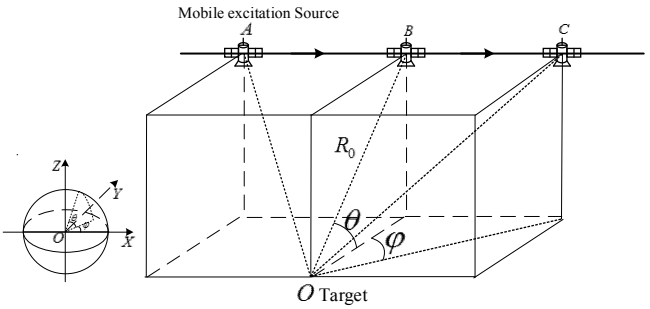

Fig.1. SAR model based on mobile excitation source

The target is located at the coordinates O . For a single target, the orbit of the spaceborne SAR can be taken as a straight line within the radar's visible range. According to the requirement of the resolution of SAR image, the target of radar

can realize the synthetic aperture along the track. The length of the synthetic aperture $L_{\max}$ can be calculated, such as (1).

$$L_{\max} = \frac{cR_0}{2f_0\rho_a} \tag{1}$$

ρ_a is the azimuthal resolution, and f_0 is the central frequency of the excitation. R_0 is a vertical distance. According to the actual work of radar, the mobile excitation source is periodically set on the line AC, and the radar will send and receive electromagnetic waves of X at a certain frequency f_{prf}. The spatial coordinates of the sampling points of the excitation source are displayed in (2).

$$\begin{aligned} x_{in} &= R_0 \cdot \cos\theta \cdot \tan\left[\varphi(t)\right] \\ y_{in} &= R_0 \cdot \cos\theta \\ z_{in} &= R_0 \cdot \sin\theta \end{aligned} \tag{2}$$

The range of variation of azimuth angle $\left[\varphi(t)\right]$ is shown in (3)

$$\left[-\arctan\frac{L_{\max}}{2R_0} : \frac{V}{f_{PRF}\cdot R_0} : \arctan\frac{L_{\max}}{2R_0}\right] \tag{3}$$

Meanwhile, the visible point coordinates of the target are established according to the occlusion relation. For the visible point $P_{visual}(n)\left(x_{visual}(n), y_{visual}(n), z_{visual}(n)\right)$, its distance to the excitation source is given by (4).

$$R_{visual}(n) = \sqrt{\begin{aligned}&\left[x_{in} - x_{visual}(n)\right]^2 + \left[y_{in} - y_{visual}(n)\right]^2 \\ &+\left[z_{in} - z_{visual}(n)\right]^2\end{aligned}} \tag{4}$$

Radar moves along the AC at speed V, the signal is emitted at t_C reaches the target Δt time later than the signal is emitted at time t_B. The position relation is shown in (5)

$$t_B + \frac{R_B}{c} + \Delta t = t_C + \frac{R_C}{c} \tag{5}$$

In (5)

$$R_C = \sqrt{\left[V(t_C - t_B)\right]^2 + (R_0\cos\theta)^2 + (R_0\sin\theta)^2} \tag{6}$$

And $R_B = R_0$, Δt is the time step in FDTD method. The quadratic equation about $(t_C - t_B)$ is obtained

$$\begin{aligned}&\left(c^2 - V^2\right)(t_C - t_B)^2 + \left(2\Delta t c^2 + 2R_0 C\right)(t_C - t_B) \\ &+2R_0 c\Delta t + c^2\Delta t^2 = 0\end{aligned} \tag{7}$$

Then get the result as

$$t_C - t_B = \frac{c(\Delta t c + R_0) + \sqrt{c\left(cR_0^2 + 2R_0V^2\Delta t + cV^2\Delta t^2\right)}}{c^2 - V^2} \tag{8}$$

Therefore, when the excitation source at the shortest distance point B is known, the electric field value of excitation source at each sampling point over the entire running track can be obtained as in (9).

$$E_{Cin}(t) = E_{Bin}(t + t_C - t_B) \tag{9}$$

Similarly, as long as the initial state of the excitation source at a certain point on the trajectory is known, the variation of this excitation source can be obtained according to the time difference between the two sampling points.

B. The near-to-far-field transformation based on surface mesh in FDTD method

FDTD algorithm calculates the near-field scattering field of target; its calculation area is divided into the following boundaries: absorption boundary, total field boundary, extrapolation surface. The Specific division of FDTD method computing space is shown in the Fig.2.

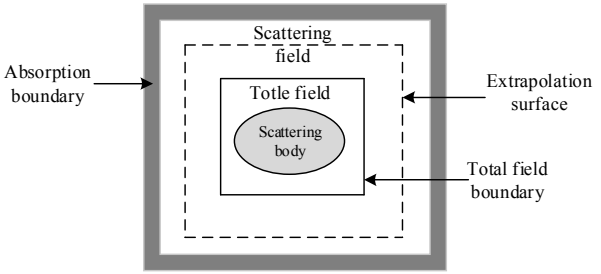

Fig.2. Regional division diagram of FDTD method

The absorption boundary is a boundary layer surrounding the FDTD calculation area, which simulates the process of absorbing divergent electromagnetic waves in a dark room in the real environment, thus limiting the calculation area to a limited space. The total field boundary divides the near field into total field area and scattering field area, and scattering field does not contain the source electromagnetic wave. After the equivalent transformation of the electromagnetic flow, the excitation source can be introduced into the total field area through the total field boundary. The electromagnetic field values in calculation area are solved iteratively in time. The iterative equation of electric field E_x is shown in (10) and (11), in which permittivity ε and permeability μ are the dielectric constants of the objects and m is the coordinate of the electromagnetic field node.

$$\begin{aligned} E_x^{n+1}\left(i+\frac{1}{2}, j, k\right) &= CA(m)\,E_x^n\left(i+\frac{1}{2}, j, k\right) \\ &+CB(m)\left[\begin{aligned}&\frac{H_z^{n+1/2}\left(i+\frac{1}{2}, j+\frac{1}{2}, k\right) - H_z^{n+1/2}\left(i+\frac{1}{2}, j-\frac{1}{2}, k\right)}{\Delta y} \\ &-\frac{H_y^{n+1/2}\left(i+\frac{1}{2}, j, k+\frac{1}{2}\right) - H_y^{n+1/2}\left(i+\frac{1}{2}, j, k-\frac{1}{2}\right)}{\Delta z}\end{aligned}\right] \end{aligned} \tag{10}$$

$$CA(m)=\frac{\frac{\varepsilon(m)}{\Delta t}-\frac{\sigma(m)}{2}}{\frac{\varepsilon(m)}{\Delta t}+\frac{\sigma(m)}{2}} \qquad CB(m)=\frac{1}{\frac{\varepsilon(m)}{\Delta t}+\frac{\sigma(m)}{2}} \quad (11)$$

In practical application, the far field information is wanted, which is calculated by near-to-far-field transformation technology in the extrapolation surface.

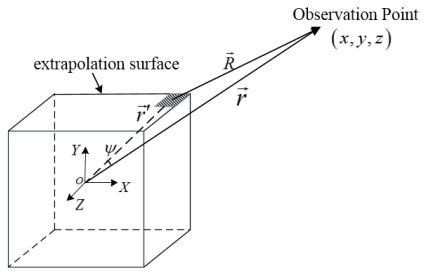

Fig.3. Calculated far field

Fig.3 shows the location relationship between Huygens surface and far-field observation point.

$$\begin{aligned} E_\theta &= -\frac{jke^{-jkr}}{4\pi r}(L_\phi+\eta_0 N_\theta) \\ E_\phi &= \frac{jke^{-jkr}}{4\pi r}(L_\theta-\eta_0 N_\phi) \end{aligned} \quad (12)$$

In (12) the vector $\vec{N}$ and $\vec{L}$ are as follows:

$$\begin{aligned} \vec{N} &= \int_S \vec{J}_s\, e^{-jkr'\cos(\psi)}dS' \\ \vec{L} &= \int_S \vec{M}_s\, e^{-jkr'\cos(\psi)}dS' \end{aligned} \quad (13)$$

In the traditional FDTD method, the extrapolated plane--Huygens plane is set as a virtual plane containing the whole target, and the result is a vector sum of the far-field electric field of entire target, which leads to the far field of the radar receiver can't represent far field characteristics of every scattering unit, as the Fig.4 shows. It needs to set a small Huygens surface for each cell that contains only one cell[7][8]. And then the electric field of each cell is pushed to the far field, which describes the scattering properties of the local target accurately.

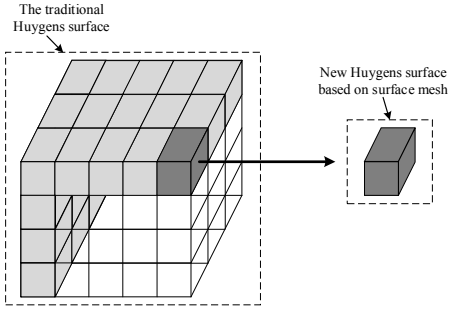

Fig.4. Schematic of Huygens surface based on surface mesh

The Huygens surface is set on the surface of each visual cell and the electric field at the observation point is deduced according to (12) and (13). The obtained far-field electric field is time-sampled with $a\Delta t$ as a time interval, Δt is the time step in FDTD and a is a constant. Then M sampling values are obtained. The electric field result is shown in (14), where $\delta(t)$ is the unit impulse function.

$$E_{farfield}(t)=\sum_{n=1}^{M}\left\{\delta\left[t-n(a\Delta t)\right]\sqrt{E_\theta^2+E_\varphi^2}\right\} \quad (14)$$

III. SAR ECHO SIMULATION METHOD

When the excitation source is at (x_{in},y_{in},z_{in}) points, as shown in (2), the distance $R_{visual}(n)$ of the visual point cell to the excitation source and the electric field $E_{farfield}(t)$ at the far-field observation point—place of radar receiver could be calculated from (4) and (14), respectively.

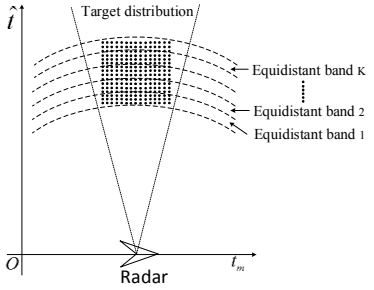

Fig.5. Division diagram of equidistant zones in target

According to the size of $R_{visual}(n)$, the visual point cells are divided into different equidistant zones, whose width is $(a\Delta t)\bullet c$, as shown in Fig.5. On the basis of the distance between equidistant zone and observation point, the number of equidistant zones is defined as $1,2,3,...,K$. The radar echoes of visible point cells within same equidistant zone reach the far-field observation point at the same time. Meanwhile, for different equidistance zone, the echoes of visible point cells are delayed for $2k\bullet(a\Delta t)$ to reach the radar receiver.

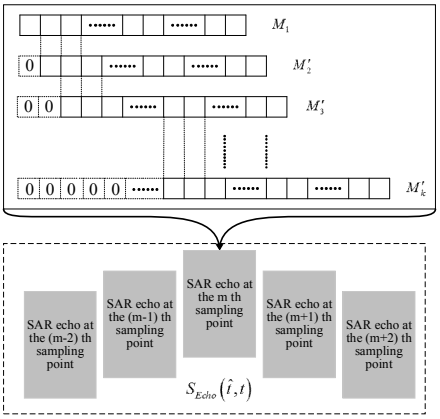

Fig.6. Echo data block handle process

Fig.6 illustrates the generating process of SAR echo. For N_k visible point cells in equidistant zone numbered k, their far-field electric field value data is a $M \times N_k$ matrix. M is the number of samples of the far-field electric field value, echoes of visible point cells within the same equidistant zone reaches the far-field observation points at the same time. Thereby, the far-field electric field values of these visual points are added correspondingly, that is, each row of the matrix is added to obtain a matrix of size $M \times 1$ denoted as M_k, which can be regarded as echo data of the target in the equidistant range k. In accordance with the above views steps, another $M \times 1$ matrix M_{k+l} is available by handle the data in equidistant zone numbered $k+l$. Compared to the equidistant zones k, the echo of visible point on equidistant zones $k+l$ arrives at the observation point for a delay of $2l \times (a\Delta t)$. Therefore, it is necessary to add the data of m row of matrix to the data of $m+2l$ row of the matrix M_k, that is, insert $2l$ zeroes before the first row of M_{k+l} to form a new matrix M'_{k+l} of size $(M+2l) \times 1$.

When the element of echo matrix $M_1, M'_2, M'_3, ..., M'_K$ is null, it will be filled zero from the first line. The echo matrix $M_1, M'_2, M'_3, ..., M'_K$ after inserting zeroes could be calculated in each equidistant zone. Finally, the echo data $S_{Echo}(t)$ at this sampling point is obtained. Similarly, the echo data obtained at each track sampling points can be got.

According to the slope distance $R(t)$ between radar and target center at each sampling point, the echo is delayed by $R(t)/2c$ to reach the receiver at each sampling point, arranged the delayed echo in parallel into a two-dimensional matrix $S_{Echo}(\hat{t}, t)$.

IV. EXPERIMENTAL RESULTS

In order to illustrate the effectiveness of the proposed method, a typical simulation experiment is carried out. The simulation parameters are as follows: radar range resolution $\rho_r = 1m$, azimuth resolution $\rho_a = 1m$, vertical distance between radar and target $R_0 = 600km$, downwards angle of antenna beam $\theta = 33^0$, radar motion speed $V = 7000\,m/s$, center frequency of excitation signal $f_0 = 1.3 \times 10^9\,Hz$, chirp rate of LFM signal $\mu = 10^{14}\,s^{-2}$, pulse repetition frequency $f_{PRF} = 1500Hz$. The following parameters can be calculated according to the above conditions. Signal bandwidth $B = 1.79 \times 10^8$, pulse width $\tau = 1.79\mu s$, synthetic aperture length $L_{\max} = 6.9 \times 10^4\,m$, azimuthal variation range $\left[-3.3^o : (4.46 \times 10^{-4})^o : 3.3^o\right]$, edge length of YEE cell $\delta = 1.9 \times 10^{-2}\,m$, time step $\Delta t = 3.7 \times 10^{-11}\,s$, time step number of iteration $Num = 4.8 \times 10^4$.

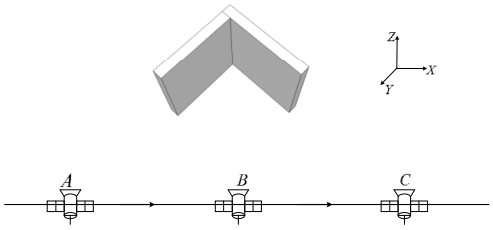

Fig.7. Dihedral corner diagram

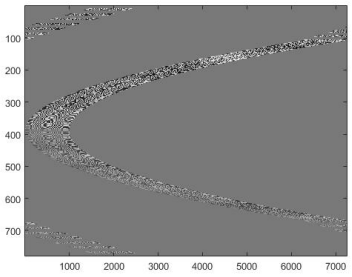

Fig.8. Echo simulated by dihedral corner

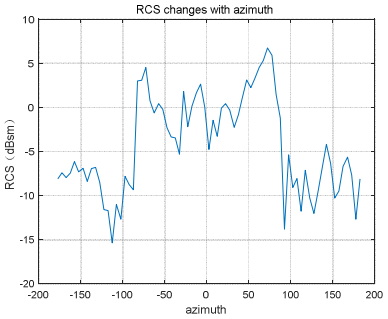

Fig.9. The change of RCS of dihedral varies with azimuth

Fig.7 shows a dihedral corner perpendicular to the XY plane, which was made of metal with an angle of 90° between the two sides. Each side was $0.5m * 0.5m$ in size. The radar was flying perpendicular to the bisector of the dihedral corner. The resulting amplitude of the echo signal is quantified as shown in Fig.8. During azimuth changed from 0° to 360°, a SAR echo simulation was performed every 5° and the target RCS at this azimuth was calculated to obtain the dihedral RCS variation as shown in Fig.9, which had a good performance of the dihedral RCS characteristics[9]. Therefore, for the sub-meter target, the proposed method could obtain high-precision echo.

Fig.10. Helicopter model

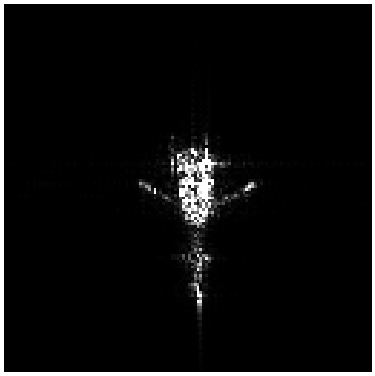

Fig.11. Imaging of helicopters SAR echo

In order to further verify the accuracy of the SAR echo, the helicopter model shown in Fig.10 was simulated by the proposed method. The imaging result according to the RD imaging algorithm was shown in Fig.11, which displayed the helicopter's contour information clearly, reflecting the edge of the aircraft information fully.

CONCLUSION

The method proposed in this paper makes full use of the accuracy of FDTD calculation, reflects the backscattering properties under different states of target realistically and the precise SAR echo data is obtained. The preliminary imaging results show that this method can not only meet the requirements of SAR system verification, but also meet the needs of high-precision simulation data in different practical applications such as high-resolution SAR imaging mode.

REFERENCES

[1] Y. Liu et al., "Echo Model Analyses and Imaging Algorithm for High-Resolution SAR on High-Speed Platform," in IEEE Transactions on Geoscience and Remote Sensing, vol. 50, no. 3, pp. 933-950, March 2012.

[2] R. T. Lord and M. R. Inggs, "High resolution VHF SAR processing using synthetic range profiling," Geoscience and Remote Sensing Symposium, 1996. IGARSS '96. 'Remote Sensing for a Sustainable Future.', International, Lincoln, NE, 1996, pp. 454-456 vol.1.

[3] G. Marino and M. Weiss, "A real time simulation model for estimation of position and orientation of two airborne SAR systems platforms inMatlab/Simulink: description," 7th European Conference on Synthetic Aperture Radar, Friedrichshafen, Germany, 2008, pp. 1-4.

[4] X. Wang, Y. Xu, Z. Ding, W. Liu, Y. Zhu and Q. Zhang, "Research on echo simulation of geosynchronous SAR," IET International Radar Conference 2015, Hangzhou, 2015, pp. 1-5.

[5] K. Wang, J. Chen, W. Yang and J. Zhou, "High accuracy SAR echo generation approach using space-time-variant backscattering characteristics," 2014 IEEE Geoscience and Remote Sensing Symposium, Quebec City, QC, 2014, pp. 656-659.

[6] T C. Ni, Q. Liu and H. Tan, "The implementation of precise delay in SAR echo simulation," 2017 International Applied Computational Electromagnetics Society Symposium (ACES), Suzhou, 2017, pp. 1-2.

[7] L. Kang, J. Lu, J. Tian, B. Zou and J. Fu, "Near-to-far-field transformation in FDTD for high resolution radar signal simulation," 2016 IEEE International Conference on Electronic Information and Communication Technology (ICEICT), Harbin, 2016, pp. 313-316.

[8] S. A. Stewart, T. J. Smy and S. Gupta, "Finite-Difference Time-Domain (FDTD) Modelling of Space-Time Modulated Metasurfaces," in IEEE Transactions on Antennas and Propagation, 2017,vol. PP, no. 99, pp. 1-1.

[9] Griesser and C. Balanis, "Backscatter analysis of dihedral corner reflectors using physical optics and the physical theory of diffraction," in IEEE Transactions on Antennas and Propagation, vol. 35, no. 10, pp. 1137-1147, Oct 1987.